Structure, Vol. 10, 1097–1106, August, 2002, ©2002 Elsevier Science Ltd. All rights reserved. PII S0969-2126(02)00805-5

Crystal Structure of the Dinuclear Zinc Aminopeptidase PepV from *Lactobacillus delbrueckii* Unravels Its Preference for Dipeptides

Daniela Jozic,[1,6] Gleb Bourenkow,[2] Hans Bartunik,[2] Henning Scholze,[3] Vincent Dive,[4] Bernhard Henrich,[5] Robert Huber,[1] Wolfram Bode,[1] and Klaus Maskos[1,6]

[1]Max-Planck-Institut für Biochemie
Abteilung Strukturforschung
Am Klopferspitz 18a
D-82152 Martinsried
Germany

[2]Unit for Structural Molecular Biology
MPG-ASMB c/o DESY
22603 Hamburg

[3]Universität Osnabrück
Fachbereich Biologie/Chemie
Barbarastraße 11
49069 Osnabrück
Germany

[4]Département d'Ingénierie et d'Etudes des Protéines
Centre d'Etudes Saclay
91191 Gif-sur-Yvette Cedex
France

[5]Fachbereich Biologie
Abteilung Mikrobiologie
Universität Kaiserslautern
Postfach 3049
D-67653 Kaiserslautern
Germany

Summary

PepV from *Lactobacillus delbrueckii*, a dinuclear zinc peptidase, has been characterized as an unspecific amino dipeptidase. The crystal structure of PepV in complex with the phosphinic inhibitor AspΨ[PO_2CH_2]AlaOH, a dipeptide substrate mimetic, reveals a "catalytic domain" and a "lid domain," which together form an internal active site cavity that traps the inhibitor. The catalytic domain is topologically similar to catalytic domains from amino- and carboxypeptidases. However, the lid domain is unique among the related enzymes. In contrast to the other related exopeptidases, PepV recognizes and fixes the dipeptide backbone, while the side chains are not specifically probed and can vary, rendering it a nonspecific dipeptidase. The cocrystallized inhibitor illustrates the two roles of the two catalytic zinc ions, namely stabilization of the tetrahedral intermediate and activation of the catalytic water molecule.

Introduction

Lactobacilli are organisms with multiple amino acid auxotrophies making them critically dependent on their ability to efficiently degrade the milk protein casein [1]. Therefore, they possess a complex proteolytic system to degrade casein to small peptides and amino acids. Since they are used as starter cultures in dairy fermentation, the quality of those dairy products depends on the distribution of the product peptides and amino acids. In view of the economic importance of those processes in the food industry, a better understanding of the proteinases involved would be highly valuable, as it would enable the development of genetically modified starter strains with improved fermentation properties. Furthermore, milk fermented by a *Lactobacillus helveticus* strain has been reported to have antihypertensive properties, rendering it interesting as functional food [2].

Dipeptidases are involved in the final breakdown of protein degradation fragments produced by other peptidases and are thus important components of the protein degradation system. Deletion of the dipeptidase *pepV* gene from *Lactococcus lactis* resulted in significantly decreased growth rates but did not reduce the final cell density [3]. The highly homologous PepV from *Lactobacillus delbrueckii* was originally described as a carnosinase cleaving the unusual peptide β-Ala-His (carnosine) [4]. It consists of a 470 residue polypeptide single chain and has been characterized as a relatively unspecific dipeptidase cleaving a variety of dipeptides, notably those with an N-terminal β-Ala or D-Ala residue, but also catalyzing the removal of the N-terminal amino acid from a few distinct tripeptides [5]. This capability led to the assignment of PepV as an aminopeptidase in addition to its predominant dipeptidase activity.

Interestingly, PepV is related not only to proteases but also to acetylornithine deacetylase and succinyldiaminopimelate desuccinylase, and has recently been described as a member of the aminoacylase-1 family [6]. These enzymes share the characteristics of hydrolyzing amide bonds in a zinc- (or cobalt-) dependent manner. Classified as a peptidase, PepV belongs to the dinuclear peptidase family M20 of clan MH [7, 8], which includes bacterial and yeast carboxypeptidases such as the glutamate carboxypeptidases G1 and G2 (CPG1 and 2) from *Pseudomonas stutzeri* and *sp*., a Gly-X carboxypeptidase from yeast, and several amino acid tripeptidases T from various bacteria [8]. Of these enzymes, a crystal structure is available only for CPG2 [9], which is of prime interest due to the enzyme's ability to cleave the C-terminal Glu from folic (pteroylglutamic) acid and folate analogs such as the chemotherapeutic agent methotrexate.

Further crystal structures of dinuclear zinc aminopeptidases are known for the M28 aminopeptidases from *Aeromonas proteolytica* (AAP)/*Vibrio proteolyticus* [7, 10] and *Streptomyces griseus* [11, 12] (clan MH) (see Figure 2A), whose catalytic domains have been shown to be related to CPG2 [9]. Further structures of dinuclear exopeptidases have been solved for leucyl aminopeptidases from bovine lens (LAP) [13–15] and *E. coli* (PepA) [16] (clan MF), the cobalt/zinc methionyl aminopepti-

[6]Correspondence: jozic@biochem.mpg.de (D.J.), maskos@biochem.mpg.de (K.M.)

Key words: dinuclear, dipeptidase, phosphinic inhibitor, zinc-metallopeptidase, aminopeptidase, aminoacylase-1 family

dases type I from *E. coli* [17] and type II from *P. furiosus* [18] and the proline-specific aminopeptidase from *E. coli* [19] (clan MG), which differ completely from the folding-type of the M20 and M28 catalytic domains, but show related zinc binding geometries. Nevertheless, none of these enzymes is a real dinuclear dipeptidase.

Here, we report the crystal structure of the dinuclear peptidase PepV, with a transition state analog, AspΨ[PO_2CH_2]AlaOH, bound to the active site to elucidate the substrate binding geometry and to identify residues critical for substrate binding and catalysis. This structure explains the preference of PepV for dipeptides, but also allows explication of the different functions of the two zinc ions.

Results

Overall Structure

468 of the 470 amino acid residues of PepV are defined in electron density. The monomeric PepV molecule assumes the shape of an extended ellipsoid, with approximate dimensions of 73 $\times$ 39 $\times$ 35 Å. It consists of two distinct domains of almost equal size: the spherical α/β-type catalytic domain coordinates the zinc and provides the "catalytic" glutamate, while the brick-shaped "lid" domain, likewise of an α/β fold, abuts the active site region of the catalytic domain with its long, small edge (Figure 1A).

The catalytic domain, formed by the first 185 and the last 83 amino acid residues, consists essentially of a twisted β sheet sandwiched between six α helices, and a second smaller three-stranded β sheet on top of this arrangement. The large sheet contains seven strands arranged in the order s1-s2-s6-s3-s7-s9-s8, with s2 representing the only antiparallel strand (Figure 1B). The active site is located at the C-terminal end of the central parallel β strands. Helix h4 is found on the back side of the central sheet, while helices h1, h2, h3, h5, and h6 cluster together on the front side, packed between the major and the minor sheet. The surface-located N-terminal helix h1 exhibits a sharp bend, while helices h3 and h6 form the domain core. The N- and the C-terminal ends are close to each other, opposite to the lid domain and the active site. The PepV catalytic domain has a fold similar to the catalytic domains of the related M20 exopeptidase CPG2 [9] and the M28 exopeptidases AAP [7] and SGAP [11] (Figure 3A). Sequence-based alignments of these catalytic domains with PepV show sequence identities of 28.1%, 19.1%, and 21%, respectively. An optimal superposition with these catalytic domains reveals that 181, 145, and 154 of the 268 PepV residues are topologically equivalent, with rms deviations of 1.58, 1.35, and 1.73 Å, respectively. Only 28.7%, 17.3%, and 20.8% of these topologically equivalent residues are identical, however (Figure 2).

CPG2 is the only structural relative in which the polypeptide chain likewise exits the catalytic domain to form another domain. The lid domain of PepV comprises the 202 residue segment Glu186-Gly387, inserted between strands s8 and s9 of the central β sheet of the catalytic domain. It consists of an eight-stranded major β sheet, a small two-stranded antiparallel sheet, two short accompanying extra strands, and four α helices. These α helices are packed in alternating orientation to the front side of the major β sheet (Figure 1C). Only the dimerization domain of CPG2 was found to be in part similar to the lid domain of PepV in a database search. The eight strands of the relatively flat major sheet are arranged antiparallel to each other in the order sXI-sI-sX-sIX-sII-sIV-sVI-sV. Both domains interact with a $\sim$500 Å^2 interface which may be described as two lateral pillars bounding the active site (Figure 1A). The left pillar is constituted by the two domain-connecting strands and surrounding side chains, while the right pillar is a mainly hydrophobic contact between the domains, but with a solvent-exposed Glu95···Arg224 salt bridge. Between these pillars, both domains form a deep cavity that accommodates the active site and the S1 and S1′ substrate binding sites (nomenclature: P1, P2, etc. and P1′, P2′, etc. represent the substrate residues in N- and C-terminal direction from the scissile peptide bond, while S1, S2, etc. and S1′, S2′, etc. correspond to subsites on the proteinase). Altogether, residues provided mainly by a number of loop segments and strands contribute to the active site. Most of these are part of the catalytic domain, but several are also provided by the lid domain (see below). The binding sites are mainly lined by the main chain segments of Gly413-Gly414-Gly415-Thr416 (the "Gly bulge"), Asp177-Ala178 and Glu153-Glu154, and by a number of charged side chains coordinating the two catalytic zinc ions or otherwise involved in the catalytic process (Figures 4 and 5).

The Active Site Cavity

The active site cavity is comparable to a tunnel, which possesses two exits toward bulk water. A smaller essentially hydrophobic exit of 3.5 Å diameter is directed toward the "front" side (in Figure 1A and to the lower left side in Figure 4), while a wider, more polar exit of 5.5 Å diameter points toward the "back" side on the molecule (in Figure 1A and to the upper right side in Figure 4). In the PepV structure, this tunnel is blocked by the phosphinic inhibitor and some water molecules. The phosphinate group represents a tetrahedral transition state analog of the scissile peptide bond of a bound substrate during hydrolysis.

In this complex, His439 Nϵ2, the O1 oxygen of the phosphinate group, one of both oxygen atoms of the 'bridging' Asp119, and one carboxylate oxygen of Glu154 coordinate zinc 1 in a first shell at an average distance of 1.92 Å. The other Glu154 carboxylate oxygen is placed more distantly (2.56 Å) (for exact distances see Figure 4A). In the inhibitor complex, the two catalytic zinc ions are placed 3.84 Å apart from each other. Zinc 2, in contrast, is more octahedrally coordinated, namely by the two carboxylate oxygens of Asp177, His87 Nϵ2, the other carboxylate oxygen of the bridging Asp119, and the N-terminal nitrogen and the other phosphinate O2 oxygen of the bound inhibitor. The larger coordination shell is reflected by an average distance of 2.13 Å and a larger variation (Figure 4A).

It is notable that the peptide group between the bridging Asp119 and the adjacent residue Asp120 exhibits a *cis*-conformation. Furthermore, the imidazole Nδ1 atoms of His439 (zinc 1) and His87 (zinc 2) are further clamped to Asn217 O and Asp89 O, respectively.

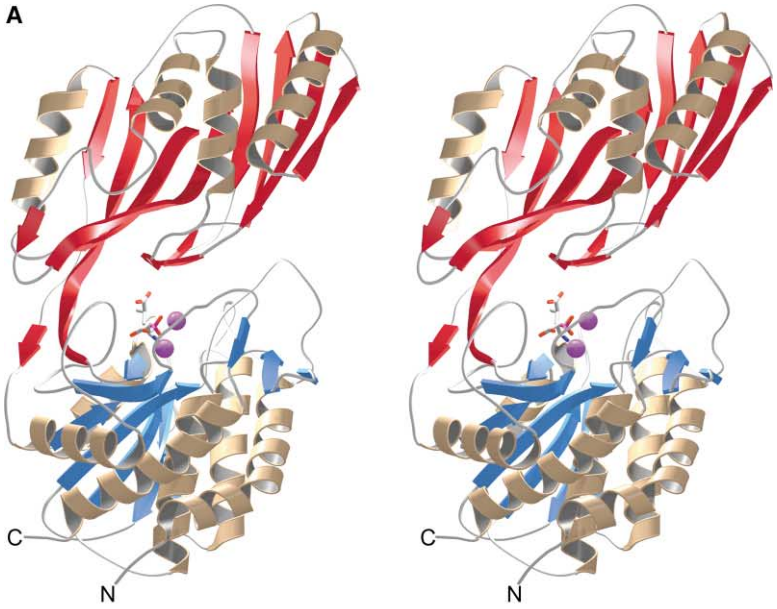

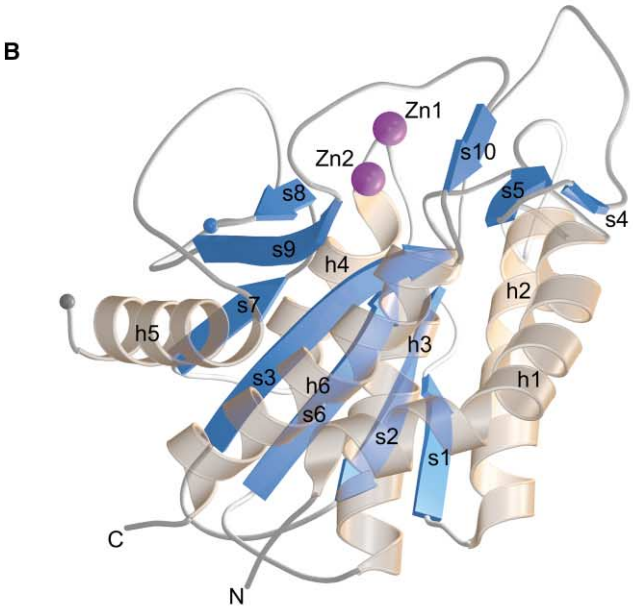

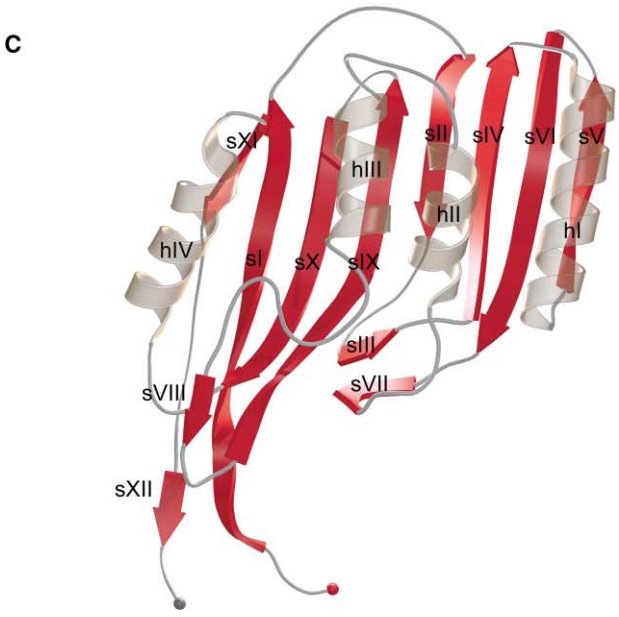

Figure 1. Ribbon Diagrams of PepV

(A) Stereo view of PepV. β sheets of the catalytic domain (bottom) and of the lid domain (top) are highlighted in blue and red, respectively. The phosphinic inhibitor AspΨ[PO_2-CH_2]AlaOH is depicted as a stick model, and the two catalytic zinc ions of the PepV active center are represented as magenta spheres.

(B) Ribbon diagram of the catalytic domain of PepV. Strands, helices, and zinc ions are labeled in their order of appearance. The blue and the gray ball indicate the end of the first part and the beginning of the second part of the catalytic domain, respectively.

(C) Ribbon diagram of the lid domain of PepV. Strands and helices are labeled in their order of appearance. The red and the gray ball indicate the beginning and the end of the lid domain, respectively.

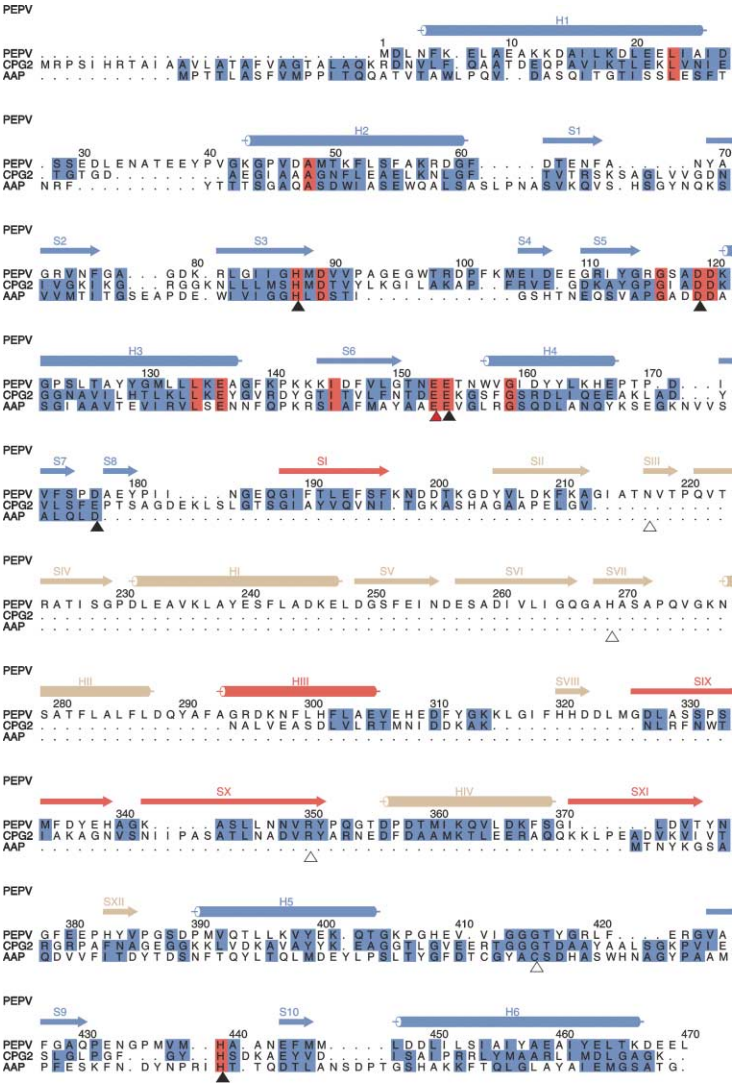

Figure 2. Structure-Based Sequence Alignment of PepV with AAP and CPG2

The secondary structural elements of PepV are shown above the amino acid sequence. The strictly conserved residues are colored in red, and similar residues are colored in blue. Strands and α helices are indicated by arrows and cylinders. Secondary structure elements present in the catalytic domains of AAP and CPG2 are shown in blue. Secondary structure elements shared between the PepV lid domain and the dimerization domain of CPG2 are shown in red, while elements only present in PepV are shown in beige. Zinc and substrate binding residues are marked by closed and open triangles, respectively. The catalytic Glu153 is highlighted by a red triangle.

The amino group of the N-terminal phosphinate inhibitor, besides interacting with its lone pair orbital with zinc 2, is directed approximately toward Asp177, forming two hydrogen bonds to its carbonyl group and to an internal water molecule (Wat1; Figure 4A). The phosphinate group "rides" on top of the (imaginary) zinc-zinc line, with the oxygens located asymmetrically on either side. The O2 oxygen is placed between both zinc ions but is significantly closer to zinc 2, and is in addition in hydrogen bond distance (2.56 Å) to one of both carboxylate oxygens of the "catalytic" Glu153 (Figure 4A). Figure 3B shows the catalytic water molecule of CPG2 next to the O2 oxygen of the PepV inhibitor, indicating that this O2 oxygen replaces presumably the catalytic water molecule in PepV. Besides its close interaction with zinc 1, the other phosphinate oxygen O1 forms two hydrogen bonds with an internal water molecule (Wat2) and with His269 Nε2. This latter imidazole is further hydrogen bonded to the Ser271 N through its Nδ1 atom (Figure 4B). His269 is therefore protonated at Nε2 and acts as a hydrogen bond donor for the phosphinate O1 oxygen. The following methylene group of the inhibitor, which mimics an sp^3 hybridized peptide nitrogen of a bound dipeptide, is 3.13 Å away from the carbonyl oxygen of Gly415 and from the "other" carboxylate oxygen of the catalytic Glu153. The C-terminal carboxylate group of the inhibitor extends into the "carboxylate groove," where it is tightly fixed by a network of hydrogen bonds with surrounding polar groups (Figure 4). This carboxylate opposes the guanidyl group of Arg350 making two short N···O charged hydrogen bonds, besides lateral hydrogen bonds formed to Gly415 N and Asn217 Nδ. The Arg350 guanidyl group is further fixed through lateral hydrogen bonds to Gly413 O and Asn348 Oδ (Figure 4).

The side chain of the AspI1 "residue" ("I" is used to refer to inhibitor residues) extends into the S1 cavity, which in PepV is of medium size. This cavity is mainly lined by hydrophobic groups such as Met436 and Met438, which also close the cavity toward the smaller front exit (Figure 4B). The AspI1 side chain does not completely fill this S1 cavity, and one of its carboxylate oxygens is in hydrogen bond distance to the Gly415 O,

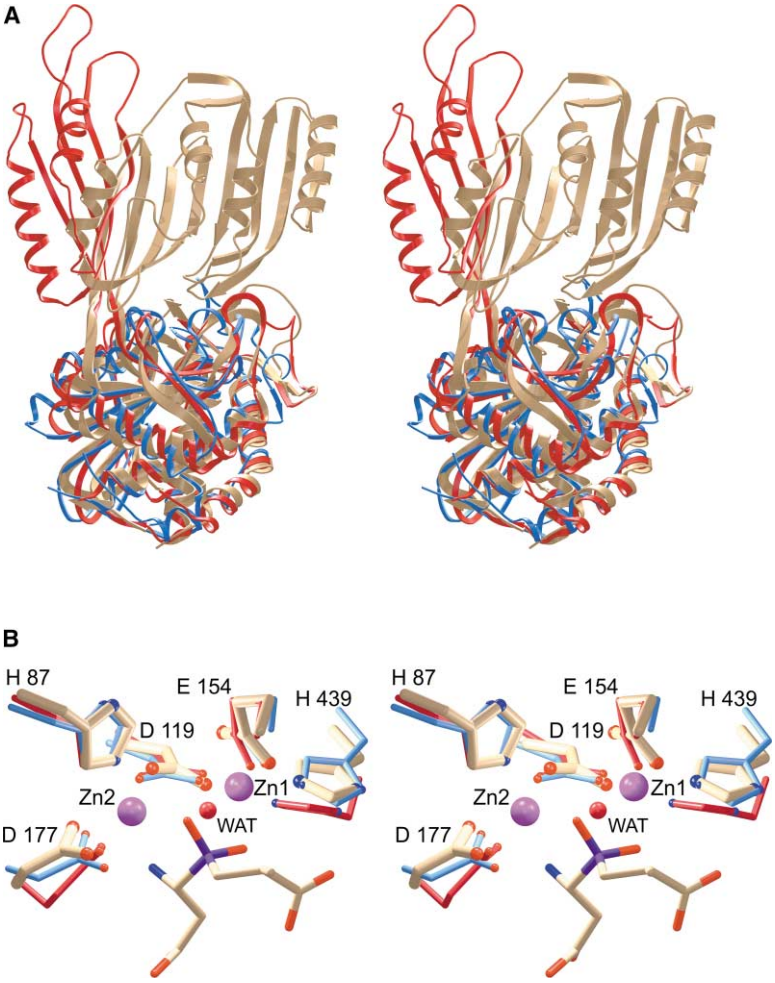

Figure 3. Superposition of PepV with CPG2 and AAP

(A) Structures were superimposed using TOP. Stereo view is shown of the superposition of PepV (beige) with AAP (blue) and CPG2 (red) after optimal fit of the catalytic domains.

(B) Stereo view of the two catalytic zinc ions, the zinc binding residues, and the inhibitor of PepV (beige) superimposed with the zinc binding residues of AAP (blue) and CPG2 (red). Residues are numbered according to the PepV sequence. The catalytic water molecule of CPG2 is depicted in red (WAT).

suggesting that this carboxylate may be protonated at the low pH (pH 5.6) of the crystal. However, a carboxylate side chain does not fit optimally. The S1 pocket seems rather to be shaped to accommodate medium-sized hydrophobic P1 side chains up to the size of a benzyl group (see also Figure 5). The AlaI2 "side chain" points into the funnel-shaped S1′ pocket that opens toward the larger back exit. This pocket is on one side hydrophobic but becomes increasingly polar toward the exit due to several carbonyl groups, the Trp157 indole moiety, and the Glu380 side chain lining it (Figure 4B).

Probable Substrate Binding

PepV shows a preference for large hydrophobic side chains, such as phenylalanine, at the N terminus of the dipeptide. On the basis of this phosphinic acid PepV complex, a Phe1-Phe2 dipeptide has been modeled into the central cavity (Figure 5). For clarity, part of the stick models covering the cavity in Figure 4B, as well as their corresponding molecular surfaces, have been removed in Figure 5. The substrate main chain interacts with the cavity residues similar to that observed for the phosphinate inhibitor chain. Therefore, the amino group should form the fifth ligand of zinc 2, and the carboxyl end should be trapped in the hydrogen bond network dominated by the Arg350 guanidyl group, both contributing to the tightening of the substrate binding. The Phe1 benzyl group would just fill the S1 cavity and could make a number of favorable hydrophobic interactions. The benzyl group of the C-terminal Phe2 residue, in contrast, would extend into the S1′ funnel-like exit where it could make many-fold contacts with surrounding groups but also with bulk water molecules.

Discussion

This structure analysis revealed that PepV is composed of a catalytic domain and a lid domain, which interact with each other and form an internal cavity at the interface. This cavity, besides providing the zinc coordinating residues, the two zinc ions, and the other substrate recognizing and active residues, leaves just enough space for the bound Asp-Ala dipeptide-like phosphinate inhibitor. The PepV catalytic domain has a fold similar to that previously found for the dinuclear carboxyl exopeptidase CPG2 [9] and for the dinuclear amino exopeptidases AAP [7] and SGPA [11] (Figure 3A). This holds even for the conserved *cis*-peptide bond between Asp119 and Asp120 (see Figure 4B), which seems to be necessary to force the important zinc bridging carboxylate into the correct geometry.

The active centers of the related dinuclear peptidases CPG2 [9] and AAP [7] are organized similar to that of PepV (Figure 3B). In both exopeptidases, zinc 1 pos-

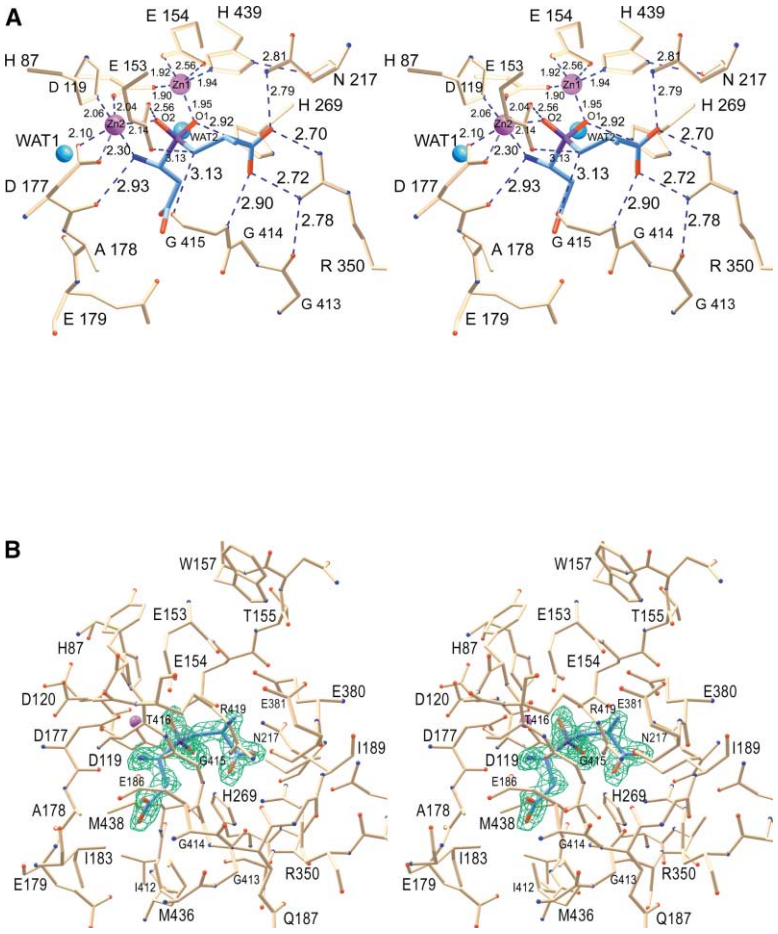

Figure 4. Stereo Close-Up View of the PepV Active Site

(A) The phosphinic AspΨ[PO_2CH_2]AlaOH inhibitor is shown in blue (carbon atoms), red (oxygens), dark blue (nitrogens), and purple (phosphorus), while the surrounding PepV residues are colored in beige (carbons). The hydrogen bonding network and the zinc interactions are shown as dotted lines, with distances depicted in angstroms. Two water molecules that take part in the interaction with the inhibitor are shown in blue.

(B) Electron density around the bound inhibitor. The inhibitor (blue) and the PepV environment (beige) are shown as stick models. The 1.8 Å $2F_o$-F_c simulated annealing omit map has been contoured at 1.3 σ.

sesses identical ligands, namely a His imidazole group, a Glu carboxylate group (in AAP less symmetrical), and one of both carboxylate oxygens of the bridging Asp residue. The zinc 2 site of AAP is virtually identical to that of PepV, with a His imidazole group, a symmetrical Asp carboxylate, the other carboxylate oxygen of the bridging Asp residue, and coordination sites for the substrate/inhibitor amino terminus and a water molecule/O2 from a phosphinate mimetic. The equivalent site in CPG2 differs slightly in that the "symmetrical carboxylate" group stems from a Glu instead from an Asp residue. A catalytic Glu residue is present in all related peptidases.

In this PepV-AspΨ[PO_2CH_2]AlaOH complex, both zinc ions are placed 3.84 Å apart from each other, while the zinc-zinc distances are slightly shorter (3.3 and 3.5 Å) in the nonliganded CPG2 and AAP. These intermetal distances seem to increase, however, upon binding of inhibitors, as exemplified for the AAP structures complexed with a hydroxamic acid inhibitor (3.7 Å) [20] or with a phosphonic acid inhibitor (3.9 Å) [10]. These data show that the active site can adapt to the respective

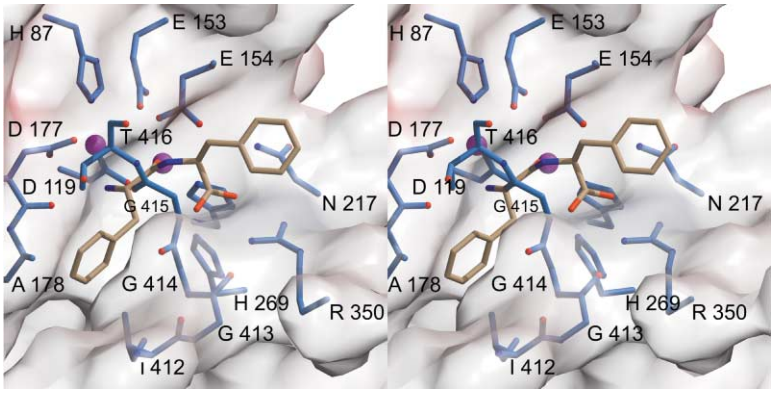

Figure 5. Stereo View of the Active Site Environment of PepV with a Modeled Dipeptide

Surface representation of the active site. Most of the lid domain and some other residues have been omitted for clarity. Only zinc binding residues and some substrate binding residues are shown in blue below and above the semitransparent surface. The modeled and energy-refined Phe1-Phe2 dipeptide is shown as a stick model in beige. The location of the Phe2 side chain in the S1′ pocket is somewhat arbitrary.

entity bound. They further support the expectation that the exact active site geometry will again slightly differ in the presence of a "real" substrate and presumably will change also in the course of a catalytic cycle.

The more distant active site environment of both exopeptidases differ, however, from that of PepV. In AAP, the Gly bulge covering the nonprimed site in PepV is replaced by a disulfide-bridged Cys residue whose carbonyl oxygen (as that of Gly415 O of PepV) points toward the position of the leaving nitrogen group. The S1 subsite of AAP, in contrast, is more restricted in size than that of PepV, while it is much larger in CPG2 (in particular due to a different arrangement of the Asp177-Ala178-Glu179 equivalent polypeptide segment), in agreement with the different specificities of these exopeptidases for P1 residues.

The lid domain of PepV is unique among the exopeptidases with respect to size and arrangement relative to the catalytic domain. Part of it (elements sI, sIX, sX, sXI, and h3 on the left side) resembles the much smaller "dimerization domain" of CPG2, which, however, extends away from the (empty!) active site of the catalytic domain [9]. Only in PepV, this extra domain folds over the active site assisting the catalytic domain to form a cavity, which harbors the S1 and the S1′ subsite. Therefore, the lid domain of PepV is uniquely involved in substrate specificity.

The Asp-Ala phosphinate inhibitor bound in this PepV complex mimics a bound dipeptide substrate at the stage of tetrahedral adduct formation, with its sp^3-methylene group of the phosphinate group resembling the protonated amide group. Therefore, this structure shows the expected interaction geometry for a dipeptide substrate when the catalytic water (or hydroxyl molecule) has attacked the carbonyl carbon of the scissile peptide bond forming a tetrahedral adduct.

In the free PepV molecule, as in other ligand-free exopeptidases such as CPG2 [9], we expect a fixed "bridging" water molecule to be placed between both zinc ions and close to the carboxylate group of the catalytic Glu153, i.e., approximately at the position of the phosphinate inhibitor O2 atom (see Figure 3B). Upon binding of the dipeptide, this water molecule will be positioned between both zinc ions and the carbonyl carbon of the scissile peptide bond. Both zinc ions, together with Glu153, will activate the bridging water, generating a hydroxyl group by proton transfer to Glu153. The carbonyl oxygen will be bound in a "oxyanion binding hole" formed by zinc 1 and the imidazole group of His269, resulting in the polarization of the carbonyl group and facilitating the nucleophilic attack of the scissile bond by the zinc-oriented hydroxyl group (positioned approximately at the O2 position) leading to a tetrahedral intermediate. This tetrahedral intermediate decays to the products, the free amino acids, after one additional proton transfer from the catalytic Glu153 carboxylate to the amide nitrogen. His269, a component of the oxyanion hole in PepV seems to have a counterpart in CPG2 (Tyr384), but none in AAP.

In dinuclear zinc peptidases, the two catalytic zinc ions seem to have different tasks [10, 15]. Zinc 1 primarily appears to facilitate substrate binding and, with His269 Nε2, to polarize the scissile carbonyl group and thereby promotes nucleophilic attack by the catalytic water molecule. On the other hand, zinc 2 seems primarily to activate the catalytic water molecule and to promote binding and hydrolysis. Therefore, the various tasks assigned to the single catalytic zinc of the mononuclear metallopeptidases might be divided effectively between the zinc ions of the dinuclear zinc peptidases, which might enhance catalytic efficiency. However, these distinct tasks of the catalytic zinc ions overlap in part in the activation of the catalytic water molecule and the stabilization of the tetrahedral state.

Table 1. Statistics of X-Ray Diffraction Data and Structure Refinement

Data Set	Edge	Peak	Remote
Wavelength (Å)	1.28210	1.28140	1.0500
Resolution (Å)	15.0–1.6	15.0–1.6	15.0–1.6
Redundancy	4.38	4.36	2.16
Unique reflections	62080	62044	62025
Completeness overall (%)	99.9	99.9	98.8
Outermost shell (%) (1.63–1.60)	99.2	99.2	93.3
I/σ	22.69	23.48	16.15
R_{sym}[a] (%)	7.6	6.8	6.1

[a] $R_{sym} = \Sigma_{hkl}\Sigma_i|I_{hkl,i} - \langle I\rangle_{hkl}|/\Sigma|\langle I\rangle_{hkl}|$

The apo form of the related AAP has been shown to bind zinc 1 first, and this mononuclear APP has been found to still exhibit 80% of the maximal hydrolytic activity of the wild-type form [10]. Therefore, a single zinc ion together with the local environment indeed seems to be capable of taking over most of the catalytic tasks of the two zinc ions present in the native state of AAP.

PepV appears to be a canonically shaped and equipped dipeptidase. The N terminus of a bound dipeptide substrate is fixed through the interaction with a carbonyl oxygen, an internal water molecule (Wat1), and zinc 2, through which the scissile peptide bond seems to be pulled in a proper position for catalysis. Preliminary model building and energy refinement experiments show that a β-Ala residue should be able to replace the AspI1 residue of the inhibitor, requiring only a slight protuberance into the S1 cavity. This is in agreement with the efficient cleavage of carnosine (β-Ala-His) and other dipeptides with an N-terminal β-Ala residue by PepV [5]. However, the cavity does not allow an N substituent, particularly not a P2 residue. The S1 pocket of PepV is shaped and lined to optimally accommodate medium-sized hydrophobic side chains, and the space around the P1-Cα atom is large enough to allow also the proper arrangement of small P1 residues with D configuration, both in fair agreement with experimental results obtained in solution [5]. The equivalent but more rigid site in AAP, in contrast, might not allow such a variability, rendering it a real aminopeptidase restricted to peptide substrates with medium-sized P1 residues of L configuration. CPG2 lacks an equivalent of the Asp177 carbonyl group, which in PepV helps to fix the amino group of the bound dipeptide. Therefore, CPG2 can bind much larger P1 equivalents such as the pteroate moiety of the predominant circulatory form of folate in mammals and its analogs used in cancer therapy such as methotrexate [9].

Table 2. Crystal Structure and Refinement Statistics

Space group	$P2_12_12_1$
Cell dimensions (Å)	a = 67.151, b = 77.025, c = 89.955
Volume fraction of protein (%)	55.24
Vm (Å^3/Da)	2.77
Total number residues	468
Total non-H atoms	3654
Number of water molecules	570
Number of zinc atoms	2
Number of inhibitor atoms	15
Temperature factors	
Protein (Å^2)	13.566
Solvent (Å^2)	27.100
Metal (Å^2)	9.185
Inhibitor	12.836
Resolution range of reflections used (Å)	15.0-1.8
R_{factor} (%)[a]	17.43
Free R_{factor} (%)[a]	20.46
Stereochemical ideality	
Bond (Å)	0.009
Angle	1.74°

[a] $R_{factor} = \Sigma|F_o - F_c|/\Sigma F_o$, where F_o is the observed and F_c is the calculated structure factor amplitude. The R_{free} was calculated for 10% of the reflections excluded from the refinement.

Furthermore, the environment around the C terminus of the bound dipeptide mimetic of PepV seems to be adapted to fix a dipeptide, with the carboxylate group framed by an extended hydrogen bond network, with the central Arg350 side chain and the Asn217 Nδ provided by the lid domain. In AAP, which lacks an equivalent to Arg350, the S1′ region is open so that substrate binding is not restricted to dipeptides but allows also binding of C-terminally elongated substrates, rendering AAP a real aminopeptidase. Free CPG2 likewise, due to the lack of a large lid domain, does not possess a direct Arg350 equivalent. However, model building studies indicate that its Arg324 side chain is in a proper position to bind and fix the C-terminal Glu carboxylate group of the folate/methotrexate substrate. There is no indication that the lid domain of CPG2 as a whole could move toward the catalytic domain.

The P1′ side chain of the bound dipeptide in the PepV enzyme-substrate complex can be of any size and charge. Tripeptides, in order to bind into the PepV active site cavity with the first residue placed in S1, could only bind after a N-Cα rotation of approximately 120°, what would place the side chain in the carboxylate groove and the third residue in the back exit. However, no side chains of a natural amino acid would fit well into the carboxylate groove, and the third residue might not find adequate binding partners. Nevertheless, certain hydrophobic tripeptides have been found to be cleaved by PepV [5], although these are few in number.

Considering the very tight packing of the dipeptidyl phosphinate inhibitor in the PepV structure, and of the dipeptide substrate in the PepV model (Figure 5), it is clear that access of these peptides to the active site cavity of PepV would benefit from a significant opening. It is conceivable that even the whole lid domain might move away form its site seen in the crystal structure to allow easier substrate access and product egress. Some conformational variability is indicated by the observation that crystals of PepV in the absence of the inhibitor diffract badly and show a much higher mosaicity.

Of particular importance in substrate binding and release seems to be the Gly bulge, which is also present in CPG2 (Figure 2A) and in SGAP (Gly-Asp-Gly), but is replaced in AAP by a more rigid disulfide bridge. This Gly bulge is fixed in the PepV complex but will presumably be more loosely arranged in the absence of a ligand. This is also suggested by the crystal structure of CPG2, in which this loop is about 0.5 Å displaced from the zinc ions in comparison to the PepV structure, and in free SGAP [11], where the equivalent Gly bulge is disordered. In addition, this Gly bulge of PepV is, through the Gly415 carbonyl group, able to orient the scissile peptide bond via hydrogen bonding to the scissile peptide amide group of a bound dipeptide substrate.

The degradation of carnosine (β-Ala-His) via PepV-like enzymes during bacterial infections might enhance the destructive potential of bacteria, because carnosine is thought to act as a physiologically important buffer of zinc ions to avoid zinc-mediated injury. Such an injury might take place on the basis of the selective inhibitory effect on N-methyl-D-aspartate NR1/NR2A receptors as well as the zinc-mediated effect on the generation of reactive oxygen species within neurons [21]. Alternatively, the protective effect of carnosine for neurons may also arise from its antiglycating activity [22].

Since mammalian carnosinases such as human serum carnosinase, which is reported to be a metalloprotease [23], are not yet well characterized, it remains a speculative suggestion that the structure of PepV shows features also of mammalian enzymes.

Biological Implications

Lactobacilli are organisms that use the milk protein casein for their growth. Therefore, they have developed a

complex proteolytic system to degrade casein to small peptides and amino acids. Their use as starter cultures for dairy fermentations makes these bacteria an important target for peptidase manipulation aimed at enhancing the quality of dairy products.

PepV is unique among its structural cognates, which include carboxypeptidases and aminopeptidases, in that it alone possesses a closed active site and is thus specialized for dipeptidase activity. The phosphinic inhibitor present in the active site shows how the C-terminal interaction of the dipeptide is utilized for the specific recognition of dipeptides without sequence specificity.

The diversity of biochemical reactions performed by aminoacylase-1 family members supports the conclusion that it is primarily the substrate binding pockets that determine which substrates are processed by a dinuclear zinc active site. The X-ray structure of PepV provides a rational framework within which mutations can be designed to engineer substrate specificity. Thus, this structure will have a significant impact on both biotechnological and fundamental aspects of this type of enzyme.

The degradation of carnosine by bacterial dipeptidases similar to PepV might also have pathological impact during bacterial infections. This hypothesis is based on the observation that carnosine can function as a buffer for zinc concentrations in tissues and, thereby, helps to protect from zinc-mediated injury, especially in the brain.

Experimental Procedures

Expression and Purification of PeptidaseV

The *pepV* open reading frame from *Lactobacillus delbrueckii* (residues Met1 to Leu470) was cloned into the BamHI and SalI restriction sites of *E.coli* expression plasmid pKV104 [5]. It was purified by a combination of anion exchange and gel filtration chromatography. Briefly, after harvesting and lysis of the cells, the crude extract was centrifuged and applied to a DE52 column (Whatman). The protein was eluted with a gradient of 0–450 mM NaCl in 10 mM sodium citrate at pH 6.0. PepV containing fractions were dialyzed against 10 mM Tris/HCl at pH 8.0 and 4°C overnight. The protein was applied to a Resource Q column (6 ml; Pharmacia, Uppsala, Sweden) and was eluted with a gradient of 0–1 M NaCl in 10 mM Tris/HCl at pH 8.0. PepV containing fractions were collected and purified on a Sephadex 75 gel filtration column (Pharmacia).

Crystallization

Crystals were grown at 18°C by the sitting drop vapor diffusion method in droplets composed of one part protein solution (25 mg/ml in 10 mM Tris/HCl at pH 8.0, 3 mM $_{(L,D)}Asp\Psi[PO_2CH_2]_{(L,D)}AlaOH$) and one part reservoir solution (0.1 M ammonium sulfate, 0.01 M $MgCl_2$, 0.05 MES/NaOH at pH 5.6, 30% PEG 8000). Due to the method of synthesis, the inhibitor used for crystallization experiments contained two asymmetric carbons which gave rise to four different compounds [24]. This mixture shows an apparent IC50 of 30 μM for PepV (data not shown). However, omit maps calculated for the inhibitor unequivocally showed only the $_{(L)}Asp\Psi[PO_2CH_2]_{(L)}AlaOH$ compound to be present in the active site of PepV (see Figure 4B), indicating that this compound possesses the highest affinity for the active site. After 2 weeks, the crystals reached a final size of 0.4 $\times$ 0.15 $\times$ 0.15 mm^3. The orthorhombic crystals are of space group $P2_12_12_1$ and contain one molecule in the asymmetric unit. For data collection, these crystals were transferred into cryobuffer (crystallization buffer with 10% [v/v] glycerol) and were frozen at 100 K.

Data Collection, Structure Solution, and Refinement

MAD data to 1.6 Å were collected from one single crystal at three different wavelengths, using synchrotron radiation at the beamline BW6 of DESY (Deutsches Elektronensynchrtron, Hamburg, Germany) with wavelengths at the ZN-K absorption edges f′ (1.2821 Å) and f″ (1.2814 Å) and one remote wavelength (1.05 Å) using a MAR-Research image plate detector (MAR Research, Hamburg, Germany). The statistics of the MAD data sets are summarized in Table 1. Complete data sets were collected through contiguous rotation ranges at a given wavelength before proceeding to the next wavelength. Rotation data were recorded in frames of 1° (high-resolution data to 1.6 Å) and 2° (low-resolution data to 2.4 Å), each through a contiguous angular range of 90° followed by another contiguous range of 90° for measuring the Friedel pairs in inverse beam geometry. The data collected at different wavelengths were processed with the programs DENZO and SCALEPACK [25], and scaled with CAD and SCALEIT from the CCP4 package [26]. Two zinc positions were localized in anomalous difference Patterson maps and were refined with MLPHARE/CCP4 [26]. After solvent flattening and density modification (DM) [27], the initial 2.0 Å electron density map was clearly interpretable and traced by a model built on Silicon Graphics (Mountain View, CA) workstations using TURBO FRODO [28]. Calculation of the electron density maps and crystallographic refinement were performed with REFMAC/CCP4 [26] and X-PLOR [29]. The refinement procedures included simulated annealing, positional refinement, and restrained temperature factor refinement using parameters of Engh and Huber [30] and maximum likelihood algorithms as provided by X-PLOR [29]. Finally, water molecules were inserted automatically and checked manually by inspection of the refinement, and individual temperatures factors were refined. The final model was refined to an R_{factor} of 17.4% (R_{free} 20.4%) for reflections from 15 to 1.8 Å (Table 2). The polypeptide chain is fully defined from Met1 to Glu468, with all main chain angles being in fully or generously allowed regions (Procheck [31]).

Searches for related structures in the database were performed using the program TOP [32]. Sequence comparisons of the aminoacylase-1 family were made using GCG [33]. Figures were drawn with MOLSCRIPT [34], Raster3D [35], and GRASP [36].

Acknowledgments

We thank Hans Brandstetter for critically reading the manuscript and valuable advice. The financial support by the SFB469 of the LM University Munich, by the "Training and Mobility" program of the European Union, and by the Fonds der Chemischen Industrie is kindly acknowledged.

Received: December 28, 2001
Revised: April 24, 2002
Accepted: May 6, 2002

References

1. Kok, J., and DeVos, W.M. (1994). The proteolytic system of lactic acid bacteria. In Genetics and Biotechnology of Lactic Acid Bacteria, M.J. Gasson, and W.M. De Vos, eds. (London: Blackie and Professional), pp. 169–210.
2. Yamamoto, N., Maeno, M., and Takano, T. (1999). Purification and characterization of an antihypertensive peptide from a yogurt-like product fermented by *Lactobacillus helveticus* CPN4. J. Dairy Sci. *82*, 1388–1393.
3. Hellendorn, M.A., Franke-Fayard, B.M., Mierau, I., Venema, G., and Kok, J. (1997). Cloning and analysis of the PepV dipeptidase gene of *Lactococcus lactis* MG1363. J. Bacteriol. *179*, 3410–3415.
4. Klein, J.R., and Henrich, B. (1998). Peptidase V. In Handbook of Proteolytic Enzymes, A.J. Barrett, N.D. Rawlings, and J.F. Woessner, eds. (London: Academic Press), pp. 1423–1425.
5. Vongerichten, K.F., Klein, J.R., Matern, H., and Plapp, R. (1994). Cloning and nucleotide sequence analysis of PepV, a carnosinase gene from *Lactobacillus delbrueckii* subsp.lactis DSM 7290, and partial characterization of the enzyme. Microbiology *140*, 2591–2600.
6. Biagini, A., and Puigserver, A. (2001). Sequence analysis of the aminoacylase-1 family. A new proposed signature for metalloexopeptidases. Comp. Biochem. Physiol. B *128*, 469–481.

7. Chevrier, B., Schalk, C., D''Orchymont, H., Rondeau, J.M., Moras, D., and Tarnus, C. (1994). Crystal structure of *Aeromonas proteolytica* aminopeptidase: a prototypical member of the co-catalytic zinc enzyme family. Structure *2*, 283–291.
8. Barrett, A.J., Rawlings, N.D., and Woessner, J.F. (1998). Introduction: clan MH containing varied co-catalytic metallopeptidases. In Handbook of Proteolytic Enzymes, pp. 1412–1416.
9. Rowsell, S., Pauptit, R.A., Tucker, A.D., Melton, R.G., Blow, D.M., and Brick, P. (1997). Crystal structure of carboxypeptidase G2, a bacterial enzyme with applications in cancer therapy. Structure *5*, 337–347.
10. Stamper, C., Bennett, B., Edwards, T., Holz, R.C., Ringe, D., and Petsko, G. (2001). Inhibition of the aminopeptidase from Aeromonas proteolytica by L-leucinephosphonic acid. Spectroscopic and crystallographic characterization of the transition state of peptide hydrolysis. Biochemistry *40*, 7035–7046.
11. Greenblatt, H.M., Almog, O., Maras, B., Spungin-Bialik, A., Barra, D., Blumberg, S., and Shoham, G. (1997). Streptomyces griseus aminopeptidase: X-ray crystallographic structure at 1.75 Å resolution. J. Mol. Biol. *265*, 620–636.
12. Gilboa, R., Greenblatt, H.M., Perach, M., Spungin-Bialik, A., Lessel, U., Wohlfahrt, G., Schomburg, D., Blumberg, S., and Shoham, G. (2000). Interactions of Streptomyces griseus aminopeptidase with a methionine product analogue: a structural study at 1.53 Å resolution. Acta Crystallogr. D Biol. Crystallogr. *56*, 551–558.
13. Burley, S.K., David, P.R., Taylor, A., and Lipscomb, W.N. (1990). Molecular structure of leucine aminopeptidase at 2.7-Å resolution. Proc. Natl. Acad. Sci. USA *87*, 6878–6882.
14. Burley, S.K., David, P.R., and Lipscomb, W.N. (1991). Leucine aminopeptidase: bestatin inhibition and a model for enzyme-catalyzed peptide hydrolysis. Proc. Natl. Acad. Sci. USA *88*, 6916–6920.
15. Sträter, N., and Lipscomb, W.N. (1995). Two-metal ion mechanism of bovine lens leucine aminopeptidase: active site solvent structure and binding mode of L-leucinal, a gem-diolate transition state analogue, by X-ray crystallography. Biochemistry *34*, 14792–14800.
16. Sträter, N., Sherratt, D.J., and Colloms, S.D. (1999). X-ray structure of aminopeptidase A from Escherichia coli and a model for the nucleoprotein complex in Xer site-specific recombination. EMBO J. *18*, 4513–4522.
17. Roderick, S.L., and Matthews, B.W. (1993). Structure of the cobalt-dependent methionine aminopeptidase from Escherichia coli: a new type of proteolytic enzyme. Biochemistry *32*, 3907–3912.
18. Tahirov, T.H., Oki, H., Tsukihara, T., Ogasahara, K., Yutani, K., Ogata, K., Izu, Y., Tsunasawa, S., and Kato, I. (1998). Crystal structure of methionine aminopeptidase from hyperthermophile Pyrococcus furiosus. J. Mol. Biol. *284*, 101–124.
19. Wilce, M.C.J., Bond, C.S., Dixon, N.E., Freeman, H.C., Guss, J.M., Lilley, P.E., and Wilce, J.A. (1998). Structure and mechanism of a proline-specific aminopeptidase from E. coli. Proc. Natl. Acad. Sci. USA *95*, 3472–3477.
20. Chevrier, B., D'Orchymont, H., Schalk, C., Tarnus, C., and Moras, D. (1996). The structure of the Aeromonas proteolytica aminopeptidase complexed with a hydroxamate inhibitor. Involvement in catalysis of the Glu151 and two zinc ions of the co-catalytic unit. Eur. J. Biochem. *237*, 393–398.
21. Boldyrev, A. (2001). Carnosine as a modulator of endogenous Zn (2+) effects. Trends Pharmacol. Sci. *22*, 112–113.
22. Boldyrev, A., Song, R., Lawrence, D., and Carpenter, D.O. (1999). Carnosine protects against excitotoxic cell death independently of effects on reactive oxygen species. Neuroscience *94*, 571–577.
23. Jackson, M.C., Kucera, C.M., and Lenney, J.F. (1991). Purification and properties of human serum carnosinase. Clin. Chim. Acta *196*, 193–206.
24. Jiracek, J., Yiotakis, A., Vincent, B., Lecoq, A., Nicolaou, A., Checler, F., and Dive, V. (1995). Development of highly potent and selective phosphinic peptide inhibitors of zinc endopeptidases 24–15 using combinatorial chemistry. J. Biol. Chem. *270*, 21701–21706.
25. Otwinowsky, Z., and Minor, W. (1993). DENZO: A FILM Processing Program for Macromolecular Crystallography (New Haven, CT: Yale University Press).
26. CCP4 (Collaborative Computing Project 4) (1994). The CCP4 suite: programs for protein crystallography. Acta Crystallogr. D *50*, 760–763.
27. Cowtan, K. (1994). Joint CCP4 and ESF-EACBM Newsletter on Protein Crystallography *31*, 34–38.
28. Roussel, A., and Cambileau, C. (1989). TURBO FRODO Version Open GI.1 (Marseille, France: Centre National de la Recherche Scientifique/Universite Aix-Marseille).
29. Brünger, A. (1992). X-PLOR Version 3.1; A System for X-Ray Crystallography and NMR (New Haven, CT: Yale University Press).
30. Engh, R.A., and Huber, R. (1991). Accurate bond and angle parameters for x-ray protein-structure refinement. Acta Crystallogr. A *47*, 392–400.
31. Laskowski, R.A., MacArthur, M.W., Moss, D.S., and Thorton, J.M. (1993). PROCHECK: a program to check the stereochemical quality of protein structures. J. Appl. Crystallogr. *26*, 283–291.
32. Lu, G.G. (2000). TOP: a new method for protein structure comparisons and similarity searches. J. Appl. Crystallogr. *24*, 946–950.
33. Wisconsin Package Version 10.0. (1999). (Madison, WI: Genetics Computer Group (GCG)).
34. Kraulis, P.J. (1991). MOLSCRIPT: a program to produce both detailed and schematic plots of protein strcutures. J. Appl. Crystallogr. *24*, 946–950.
35. Meritt, E.A., and Murphy, M.E.P. (1994). Raster3D version-2.0: a program for photorealistic molecular graphics. Acta Crystallogr. D Biol. Crystallogr. *50*, 869–873.
36. Nicholls, A., Sharp, K.A., and Honig, B. (1991). Protein folding and association: insights from the interfacial and thermodynamic properties of hydrocarbons. Proteins *11*, 281–296.

Accession Numbers

The coordinates have been deposited at the Protein Data Bank under the accession number 1LFW.